

Check for updates

Original Article



Prediction of thermally induced postbuckling of clutch disks using the finite element method

Zhuo Chen^{1,2}, Yun-Bo Yi² and Ke Bao³

Proc IMechE Part J:
J Engineering Tribology
2021, Vol. 235(2) 303–314
© IMechE 2020
Article reuse guidelines:
sagepub.com/journals-permissions
DOI: 10.1177/1350650120901978
journals.sagepub.com/home/pij



Abstract

Buckling and postbuckling of automotive clutch disks can be excited by the temperature fields caused by frictional heat generation during engagement of clutch systems. Linear and nonlinear buckling finite element analyses are performed to evaluate the thermal postbuckling of clutch metal disks. The dominant buckling modes are first obtained through performing linear buckling finite element analysis (FEA) analyses. The scaled displacement fields obtained from the linear buckling FEA analyses are added to the original geometries to generate the perturbed meshes. The postbuckling is then investigated by performing nonlinear buckling FEA analyses. The commercial FEA software ABAQUS is used in the current study. The effects of the temperature-dependent material properties are studied. It is concluded that the temperature dependence of material properties affects the postbuckling behaviors significantly.

Keywords

Buckling, postbuckling, finite element method, eigenvalue, clutch disks

Date received: 20 September 2019; accepted: 26 December 2019

Introduction

During engagement of automotive clutch systems, a large amount of heat can be generated, and the temperature of clutch systems can be raised significantly. In the presence of excessive hoop stresses caused by thermal expansion, the metal disks of multidisk clutch systems can buckle laterally. Due to its importance in industrial applications, a large amount of conventional thermal buckling analyses (i.e. linear buckling analyses) on clutch disks are reported in the literature. Through applying Timoshenko's beam theory, Audebert et al.² inspected the thermal buckling phenomenon caused by residual stresses of disk plates. The influences of geometric parameters and material properties on this phenomenon were studied by Ma.³ Through conducting experiments, Xiong et al.4 proved that Timoshenko's beam theory is applicable to evaluate the thermal buckling of clutch disks. These two groups of researchers found that the dominant buckling modes of clutch disks can be either axisymmetric or non-axisymmetric.^{3,4} Based on the firstorder and higher-order shear deformation theories, Najafizadeh and Hedayati⁵ and Najafizadeh and Heydari⁶ performed analyses on the thermal buckling of circular disks. Zhao et al.7 assessed the effects of multiple thermal loads with different profiles on the thermal buckling of clutch disks. It was found that the profiles of thermal loads impact the thermal buckling deformation fields. Chen et al.⁸ revealed the existence of the coupling between thermoelastic instability and thermal buckling in multidisk clutch systems.

The behavior of a structure after it buckles is named as "postbuckling." The conventional buckling finite element analysis or *linear* finite element buckling analysis can merely estimate the buckling deformation modes and the associated critical buckling loads. The postbuckling or *nonlinear* buckling analysis is also able to investigate the displacement field at a particular loading condition. Ma and Wang⁹ and Li et al. ¹⁰ investigated thermal postbuckling of functionally graded material circular plates by applying von Karman's plate theory. Sepahi et al. ¹¹ inspected the axisymmetric postbuckling of an annular plate which is fixed in both inner and outer radii by using the first-order shear deformation theory.

Corresponding author:

Zhuo Chen, Henan University of Technology, 100 Lianhua Road, Zhengzhou, Henan 450001, China. Email: zhuochen1985@hotmail.com

¹School of Mechanical and Electrical Engineering, Henan University of Technology, Zhengzhou, China

²Department of Mechanical and Materials Engineering, University of Denver, Denver, USA

³China North Vehicle Research Institute, Beijing, China

To the authors' knowledge, the thermal postbuckling of clutch disks has not been investigated systematically. One obvious defect of the existing models is that the boundary conditions were not precisely represented. In real applications, only the inner or the outer radius of a clutch disk is constrained, but not both. Multiple researchers pointed out that the boundary condition affects both the buckling modes and the associated critical buckling temperatures.^{7,8} Thus, the first purpose to perform the current analysis is to investigate the effects of the boundary condition. The second motivation to perform the current analysis is that the previous works focused on the axisymmetric modes alone. 9-11 However, the non-axisymmetric modes can be dominant in some situations, and therefore evaluating the axisymmetric modes alone could be inadequate.12

Method

Principle of nonlinear buckling analysis

As shown in Figure 1, the current study consists of two consecutive steps. The first step contains linear buckling analyses from which the dominant buckling deformation modes and the corresponding critical buckling temperatures are obtained. Moreover, the scaled deformation fields of the dominant buckling deformation modes extracted from the results of the first step are then used as the initial perturbations in the second step. In the second step, nonlinear buckling analyses are subsequently conducted to investigate the postbuckling behaviors of clutch disks.

The linear buckling analysis is performed by using the commercial software ABAQUS. The geometric representation, material properties, boundary condition, and reference load are defined in the graphic interface of ABAQUS. The "BUCKLE" analysis module that is capable of computing the critical buckling eigenvalues and the corresponding buckling deformation modes is applied. The governing equation for the buckling of a mechanical structure is

$$([K] + \lambda_{cr}[K_{\sigma}]_{ref})\{\delta D\} = \{0\}$$

$$(1)$$

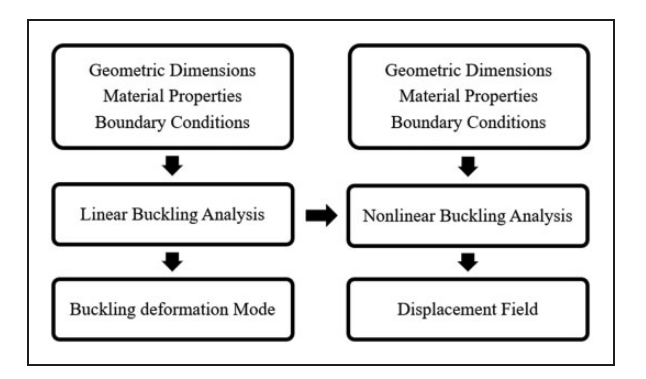


Figure 1. The flowchart of a postbuckling analysis.

where $[K_{\sigma}]_{ref}$ represents the stress stiffness matrix induced by the reference load, λ_{cr} is the critical buckling eigenvalue, and the vector $\{\delta D\}$ contains the buckling displacement field. ^{13,14} In comparison with the radial dimension, the thickness of a clutch disk is negligible. Therefore, the eight-node shell elements with reduced integration are used to develop the FEA model. The finite element model and its corresponding mesh are shown in Figure 2.

It is necessary to mention that the results of linear buckling analyses in ABAQUS are critical buckling eigenvalues. Moreover, the critical buckling loads are the products of the critical buckling eigenvalues and the reference loads. For an annular disk, all buckling modes can be classified into two types: the *coning* modes and the *wavy* modes.³ A coning mode is an out-of-plane mode that is axisymmetric. However, the wavy mode has multiple reversals in the circumferential direction.^{3,15} To extract the displacement field of the dominant buckling mode, the ABAQUS keyword "*NODE FILE*" has been inserted to the input script file manually.

The linear buckling analysis in ABAQUS is indeed a type of eigenvalue algorithm. It is only capable of determining the stability boundaries of mechanical structures. If the load–displacement response is of interest, a nonlinear buckling analysis must be performed. The governing equation defining the nonlinear buckling problem of a structure is

$$([K] + [K_{\sigma}] + [K_L])d\{\delta D\} = d\{P\}$$

$$(2)$$

where the matrix $[K_L]$ is caused by a large displacement and is called as *initial displacement matrix*, and $d\{P\}$ and $d\{\delta D\}$ represent the incremental load and the incremental displacement, respectively.¹⁶

The "RIKS" analysis step in ABAQUS is adopted to simulate the postbuckling behaviors of a clutch plate. This method has been widely used to analyze postbuckling behaviors of various structures. ^{17,18} The nonlinear buckling model can be modified from the linear buckling FEA model by replacing the "BUCKLE" analysis step with a "RIKS" analysis

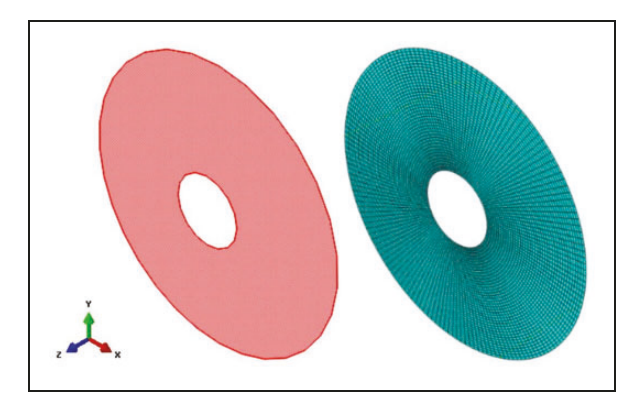


Figure 2. A clutch disk model and its corresponding mesh.

step. It should be noticed that the load defined in a nonlinear buckling model is the *critical buckling load* which is equal to the product of the critical buckling eigenvalue and the reference load defined in the linear buckling analysis. To add the scaled deformation field of the dominant buckling mode to the original geometry of the clutch plate as an initial perturbation, the keyword "*IMPERFECTION*" is manually added to the ABAQUS input file. As the maximum nodal values of the displacement fields obtained from the linear buckling analyses are normalized to unit values in the ABAQUS results, the displacement fields should be multiplied by a scaling factor. The effect of the scaling factor will be discussed in the following section.

Method of verification

As the convergence study and verification of linear buckling analyses have been elaborated in Zhao et al.⁷ and Chen et al.,¹⁵ only the validation process of the method is presented in this section. The numerical results obtained by applying the method described in the previous section are compared with the results presented in Sepahi et al.¹¹ In order to do so, the geometric parameters used in Sepahi et al.¹¹ are chosen for the verifying purpose. The boundary condition is specified in such a way that the inner and outer radii are simply supported. The material properties are temperature-independent. The geometric dimensions and material properties presented in Sepahi et al.¹¹ are listed in Table 1.

The temperature distribution in Sepahi et al.¹¹ is governed by the one-dimensional steady-state conduction equation

$$\frac{d}{dr}\left(r\frac{dT}{dr}\right) = 0\tag{3}$$

As a result, the temperature distribution along the radial direction is

$$\begin{cases} T(r) = T_a - \Delta T \frac{\ln\left(\frac{r}{r_a}\right)}{\ln(r_b/r_a)} \\ \Delta T = T_a - T_b \end{cases}$$
 (4)

where T_a is the temperature at the inner radius and T_b is the temperature at the outer radius. ¹⁹ According to Sepahi et al., ¹¹ the annular disk buckles when T_a and T_b are equal to 26.85 and 138.33 °C, respectively. Therefore, the thermal load in the linear buckling

analysis is set as

$$T(r) = 26.85 - (26.85 - 138.33) \frac{\ln \frac{r}{25}}{\ln 4}$$
 (5)

The eigenvalue obtained from the model constructed by S8R elements is 0.9325, which implies that the difference is around 6.75%. Considering that the result in Sepahi et al. 11 is obtained through a two-dimensional analytical model, this difference is acceptable. The dominant buckling mode is an axisymmetric mode which is shown in Figure 3. In Figure 3, the nodal displacements in the axial direction are dimensionless. As shown in the colormap, the maximum of the nodal displacements has been normalized to a unit value and is represented by red. Moreover, as the inner and outer radii are constrained, the nodal displacements are 0, and those two regions are represented by blue.

As mentioned previously, the scaled displacement field should be added to the original geometry as an initial perturbation. A small scaling factor is preferred, as an excessive perturbation can change the geometry visibly, leading to an inaccuracy in the result. However, if the scaling factor is smaller than a critical value, the numerical oscillations would cause a divergence in the result. The postbuckling of a certain structure probably involves multiple *critical points* where the structure cannot sustain any increase of the applied load. Therefore, Newton's method in which either the load or the displacement is selected as the independent variable is not appropriate for simulating postbuckling problems. In ABAQUS, the *arc length* method in which a third variable *arc length* is

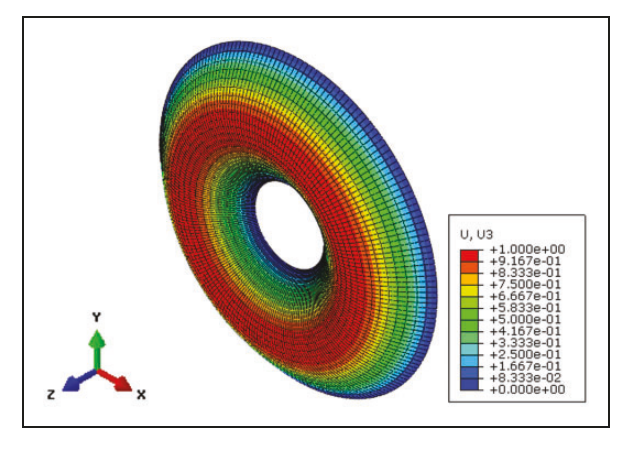


Figure 3. The dominant mode of the postbuckling model.

Table 1. Geometric dimensions and material properties of verification model.

Inner radius r_a (mm)	Outer radius r_b (mm)	Thickness (mm)	Young's modulus (GPa)	Poisson's ratio	Thermal expansion coefficient (K^{-1})
25	100	2	348	0.24	5.8723 × 10 ⁻⁶

used to determine the load increment and displacement increment simultaneously is applied to perform postbuckling analyses. More comprehensive reviews of arc length method can be found in Riks. ABAQUS is capable of plotting the *load proportionality factor* (LPF) versus the *arc length*. In the rest of the current study, we call this type of diagram as *load history diagram* which represents how the load has been applied to the structure incrementally.

Figure 4 shows a comparison between the load history diagrams of the model with 0.1% perturbation (i.e. the largest value of the perturbation is equal to 0.1% of the thickness of the plate) added to the original configuration and that of the model with 1% perturbation added to the original configuration. The horizontal axis in the above figure is the arc *length*, which represents the computational increment. The vertical axis of Figure 4 is the LPF, which is a normalized value. A unit value of LPF denotes that 100% of the defined load has been applied to the structure. The threshold of the curve represents the simulated critical buckling load. Through this figure, it can be concluded that the calculated critical buckling temperature obtained from the model with 0.1% perturbation is about 95% of the value obtained from the linear buckling analysis. It also shows that an excessive perturbation (1%) can reduce the simulated critical buckling temperature significantly. Theoretically, as the scaling factor decreases, the load history curve will be finally with a " Γ " shape. However, it is found that when the perturbation is less than 0.1% $(2 \times 10^{-3} \text{mm})$, the results started to diverge.

As shown in Figure 5 and Table 2, the dimensionless displacements in the axial direction at the medium radius $(r_m = (r_a + r_b)/2)$ under multiple temperature

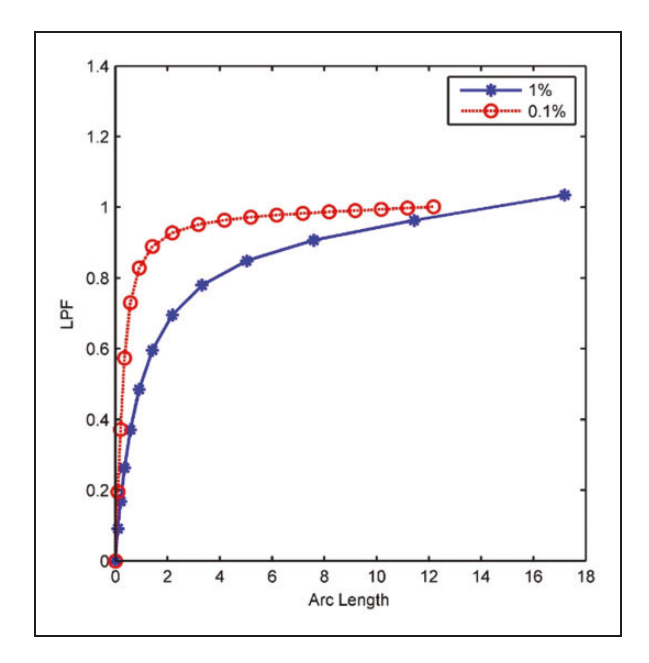


Figure 4. Load history diagrams obtained from models with different perturbations.

differences computed through the finite element method have been compared to the results reported in Sepahi et al.¹¹ It shows that the average error is around 5.67%, which is acceptable for the current study.

Results

Linear buckling analysis

Multiple models with different geometric parameters are developed in the current research. In each model, either the outer radius or the inner radius is constrained. It is assumed that these two types of clutch disks are made of the same kind of material. The material properties and geometric dimensions are listed in Table 3.

In the current study, the thermal loads are assumed as linearly increasing from the inner radii to the outer radii of the annular plates, which is based on the fact that frictional heat generation is proportional to the relative sliding speeds in automotive clutch systems. The thermal loads can be represented by the following equations

$$\begin{cases}
T(r) = \Delta T \frac{r - r_a}{r_b - r_a} \\
\Delta T = T_b - T_a
\end{cases}$$
(6)

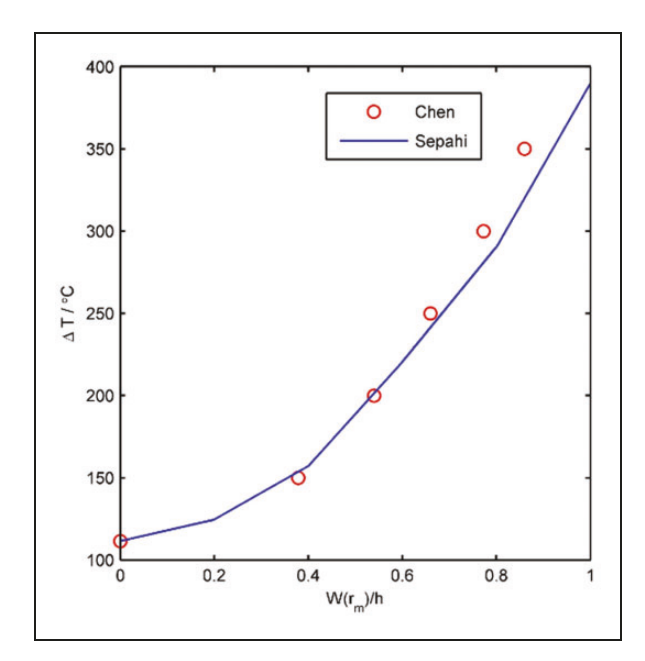


Figure 5. Verification results.

Table 2. Comparison between simulation results and analytical solutions.

ΔΤ	150	200	250	300	350	400
Sepahi	0.370	0.520	0.710	0.820	0.921	1.020
Chen	0.379	0.540	0.660	0.773	0.860	0.935

	• •					
	Inner radius	Outer radius	Thickness	Young's modulus	Poisson's ratio	Thermal expansion
Disk I						
Symbol	R_{al}	R_{b1}	h_1	Eı	v_1	α_{I}
Unit	mm	mm	mm	GPa	N/A	$10^{-6}/K$
	86	125	2.25	160	0.29	12.7
Disk 2						
Symbol	R_{a2}	R_{b2}	h ₂	E_2	v_2	α_2
Unit	mm	mm	mm	GPa	N/A	$10^{-6}/K$
	44.5	57	3.25	160	0.29	12.7

Table 3. Material properties and dimensions of the models.

Table 4. The results of linear buckling analysis.

BC Result				
(°C)	SF	CF	FS	FC
Disk I	-31.0	420.8	31.1	749.0
Disk 2	-381.3	6819.3	475.0	14,165

BC: boundary condition.

In the linear buckling analyses, i.e. the first step, ΔT is set as 1 °C. Therefore, the critical buckling temperatures are equal to the calculated critical buckling eigenvalues. It should be mentioned that in a linear buckling FEA analysis the critical buckling load is the product of the applied mechanical or thermal reference load and the calculated critical buckling eigenvalue. The calculated critical buckling temperatures are tabulated in Table 4 in which the boundary conditions are presented in a simplified fashion. In Table 4, SF represents that the inner radius is simply supported and the outer radius is free, whereas FS represents that the inner radius is free and the outer radius is simply supported. In the FC boundary condition, the inner radius is free and the outer radius is clamped. Moreover, in the CF boundary condition, the inner radius is clamped and the outer radius is free.

Through Table 4, it can be concluded that the models of Disk 1 with the CF and FC boundary conditions and the model of the Disk 2 with the FS condition are of practical importance, as the operating temperatures of clutch systems are usually well below 1000 °C and positive. Hereafter, these three models are named as models 1, 2, and 3, respectively. The dominant buckling modes of model 1 and model 2 are wavy modes, and the dominant buckling mode of model 3 is a coning mode. These models are selected in the current research to investigate the postbuckling behaviors. The dominant buckling modes of these three models are shown in Figure 6, in which the red zones represent larger nodal displacements in the axial direction and the blue zones represent smaller nodal displacements in the axial direction. It shows that the dominant mode of model 1 is a sixth-order wavy mode (i.e. there are six zones with large displacement), the dominant mode of model 2 is a fourth-order wavy mode, and the dominant mode of model 3 is a coning mode.

Postbuckling analysis

To perform a postbuckling analysis for a specific structure, the scaled displacement field obtained from a linear buckling analysis must be added to the original geometry as an initial perturbation. The value of the scaling factor should be tested carefully, as an excessive perturbation can change the original geometry and hence the simulated results. The scaling factor can be determined through the load history diagrams. The load history diagrams of model 1, model 2, and model 3 with 0.1 and 1% initial perturbations are shown in Figure 7.

If the material properties are temperature-independent, the thresholds of the load history diagrams should be close to the unit values on the vertical axes which correspond to the critical buckling temperatures obtained from the linear buckling analyses. Through Figure 7, it can be found that the thresholds of the load history diagrams of the models with 0.1% perturbations are close to the unit values. The slight differences are caused by the geometric nonlinearity and numerical errors. However, there are no obvious thresholds in the load history diagrams of the models in which the perturbations are equal to 1% of the disk thicknesses, which implies that the results are less accurate. In the rest of the current study, the values of the perturbations applied to the models are equal to 0.1% of the disk thicknesses.

The displacement profile in the axial direction along the outer radius of model 1 and the displacement profile in the axial direction along the inner radius of model 2 at the two different levels of temperature: (1) the critical buckling temperatures and (2) 100 °C above the critical buckling temperatures are shown in Figure 8. In the figure, it shows that at the critical buckling temperature the largest displacement in the axial direction along the outer radius of model 1 is around 0.3 mm, and the largest

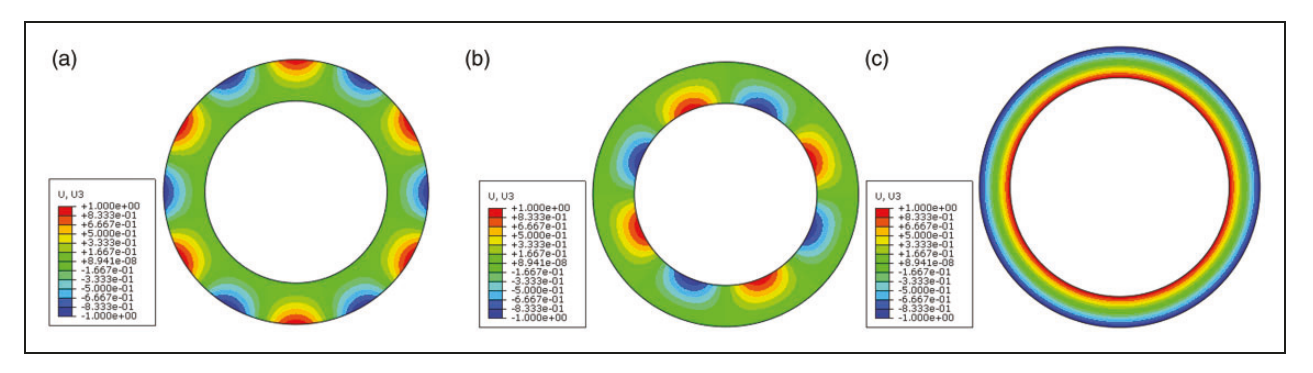


Figure 6. Dominant buckling modes. (a) Model I, (b) model 2, and (c) model 3.

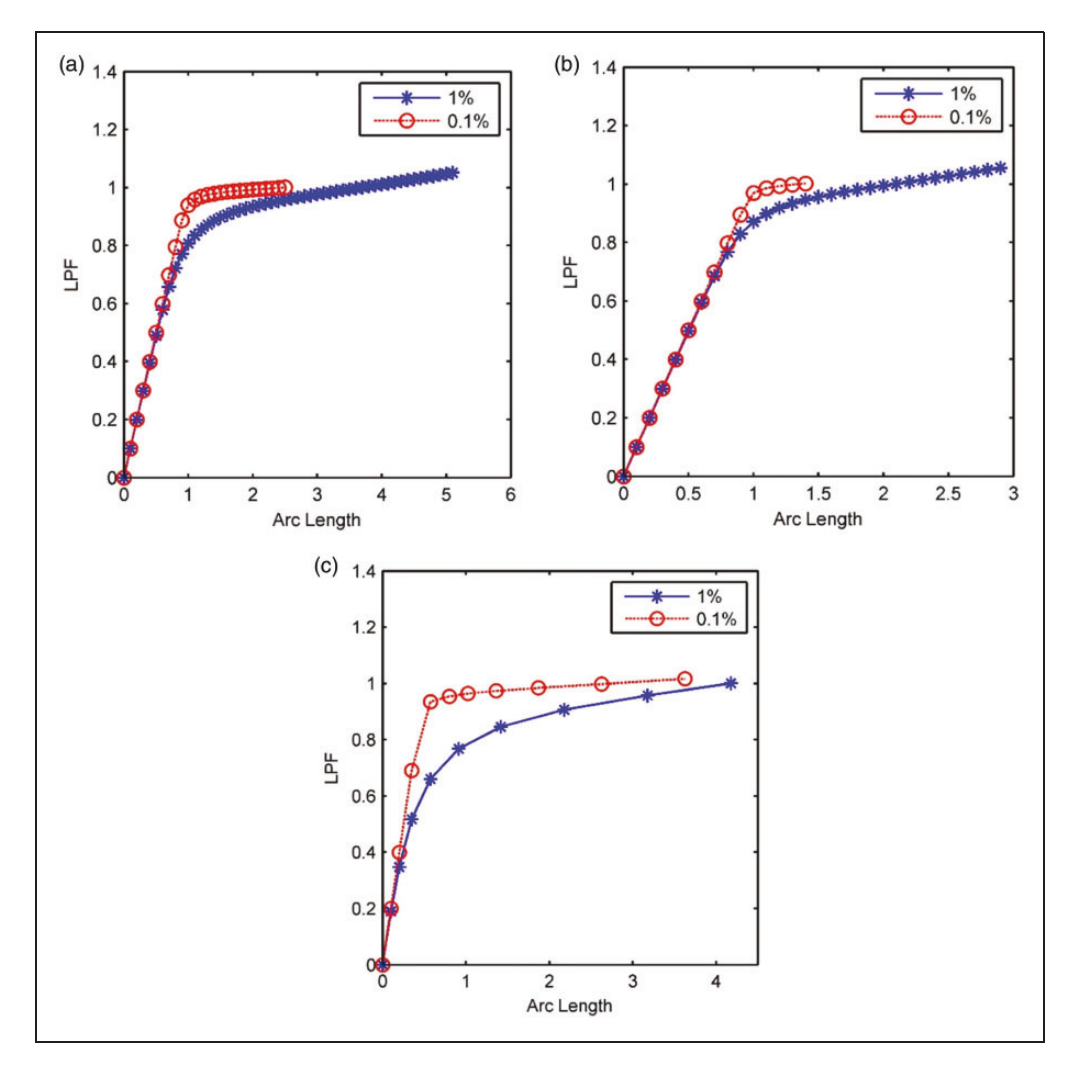


Figure 7. Load history diagrams with different initial perturbations. (a) Model I, (b) model 2, and (c) model 3. LPF: load proportionality factor.

displacement along the outer radius of model 1 at 521 °C (i.e. 100 °C above the critical buckling temperature) is around 1.6 mm. It also shows that at the critical buckling temperature the largest displacement in the axial direction along the inner radius of model 2 is around 0.2 mm, and the largest displacement along the inner radius of model 2 at

850 °C (i.e. 100 °C above the critical buckling temperature) is around 2 mm. The largest displacement in the axial direction of model 1 at 800 °C is compared to the result of model 2 at 800 °C. It is found that at 800 °C, the largest displacement in the axial direction of model 1 is around 2.4 mm, and the largest displacement in the axial direction of model 2 is around

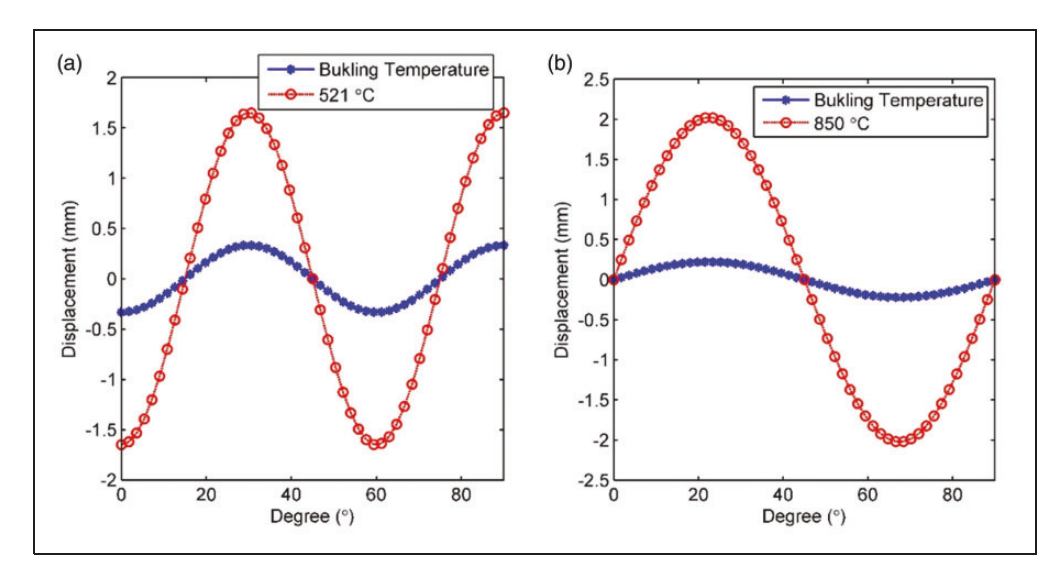


Figure 8. (a) The displacement in axial direction at the outer radius of model 1 and (b) the displacement in axial direction at the inner radius of model 2.

1.8 mm. Hence, fixing an annular disk at outer radius is a preferred boundary condition in practical clutch applications due to its higher critical temperature and smaller deformation.

The displacement distributions in the axial direction along the radius of model 3 at the critical buckling temperature and 100 °C above the critical buckling temperature are shown in Figure 9. The figure shows that the largest displacement in the axial direction at the critical buckling temperature is around 0.4 mm, and the largest displacement in the axial direction at 575 °C (i.e. 100 °C above the critical temperature) is around 1.1 mm. The relatively small deformation is probably due to the large thickness and small radial width. To verify this assumption, the boundary condition of model 2 is changed to FS and the nonlinear buckling analysis is performed. It is found that at the temperature 100 °C above the critical buckling temperature (i.e. 131 °C), the largest displacement in the axial direction is around 2.8 mm. Therefore, it is concluded that the FS boundary condition is less favorable, as it induces a lower critical buckling temperature and a larger deformation.

Effects of temperature-dependent material properties

In this section, the effects of the temperature-dependent material properties are studied. In general engineering applications, the relationship between the elastic modulus of a certain type of metal and temperature can be estimated by the following equation²¹

$$E(T) = E_0[1 + \alpha_E(T - T_0)] \tag{7}$$

where E(T) represents the elastic modulus at a specific temperature T, E_0 is the elastic modulus at the

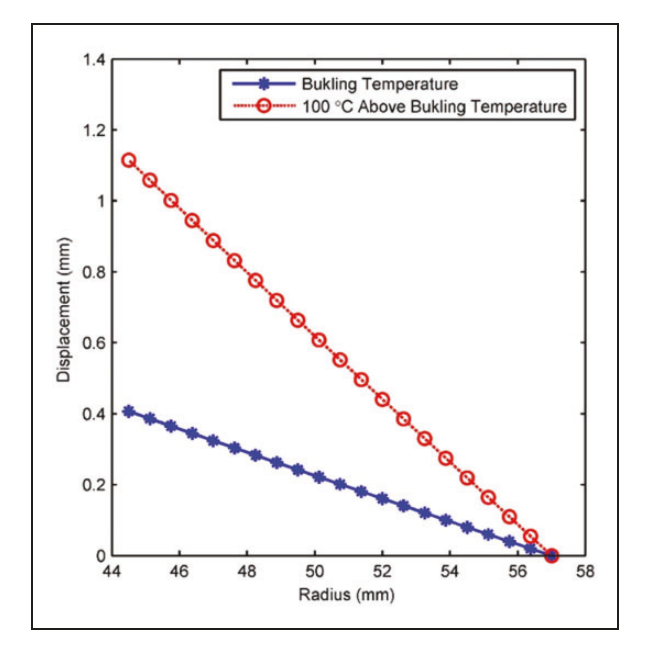


Figure 9. The displacement in the axial direction along the radius of model 3.

reference temperature T_0 , and α_E is the temperature coefficient of elastic modulus. Based on Liu and Liu, ²² the value of α_E can be selected as -0.35×10^{-3} /°C. The Young's moduli in the three models are set as temperature-dependent, and the other properties remain the same. The load history diagrams with and without the temperature dependence are compared in Figure 10. It is found that Young's modulus does not affect the critical buckling temperature significantly in general. For model 1 specifically, the critical buckling temperature obtained from the FEA model with temperature-dependent Young's modulus is slightly higher than the value obtained from the FEA model with temperature-independent Young's modulus, as the threshold of the load history diagram

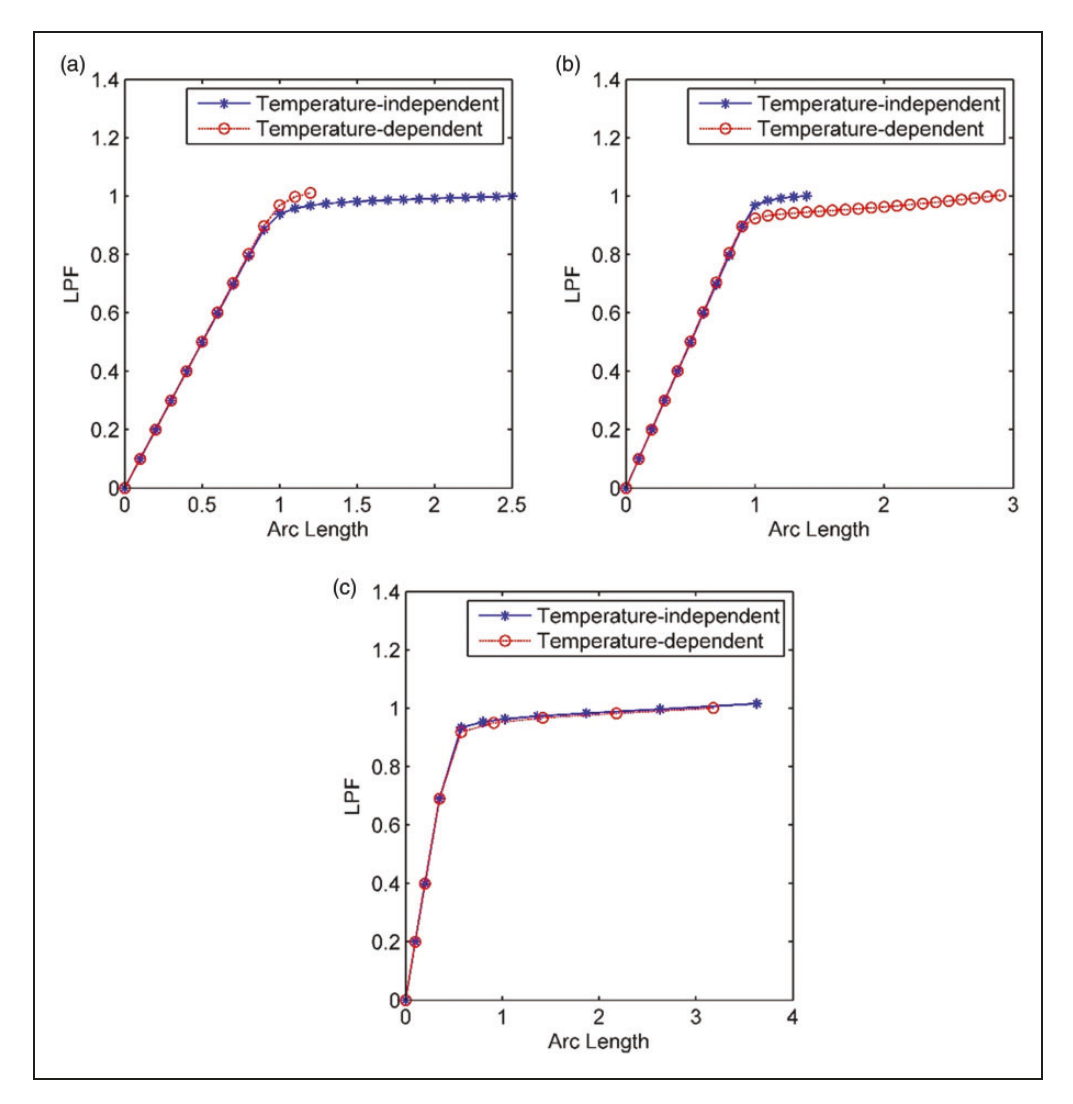


Figure 10. The load history diagrams of models with temperature-dependent Young's moduli. (a) Model 1, (b) model 2, and (c) model 3.

LPF: load proportionality factor.

of the model with temperature-dependent Young's modulus is slightly higher, whereas the critical buckling temperature obtained from model 2 with temperature-dependent Young's modulus is slightly lower than the value obtained from the FEA model with temperature-independent Young's modulus. It also reveals that the critical buckling temperature of model 3 does not change obviously, since the two load history diagrams overlap with each other.

The relationship between the thermal expansion coefficient of a particular type of metal and temperature can be described by the following equation²²

$$\alpha(T) = a[1 + b(T + 273.15)] \tag{8}$$

where a and b are constants. The values of a and b are selected as 9.567×10^{-6} and 1.115×10^{-6} based on literature.²² Therefore, the relationship between the

expansion coefficient and temperature can be described by the following equation

$$\alpha(T) = 9.567 \times 10^{-6} [1 + 1.115 \times 10^{-6} (T + 273.15)]$$
(9)

The thermal expansion coefficients in the models are set as temperature-dependent, and the other properties remain unchanged. The load history diagrams with and without the temperature dependence are compared in Figure 11. Through the figure, it shows that the critical buckling temperatures represented by the thresholds of the load history diagrams with temperature-dependent thermal expansion coefficients are around 80% of the values obtained from the linear model.

As shown in Figure 12, if both Young's moduli and expansion coefficients are set as temperaturedependent, it is found that the critical buckling

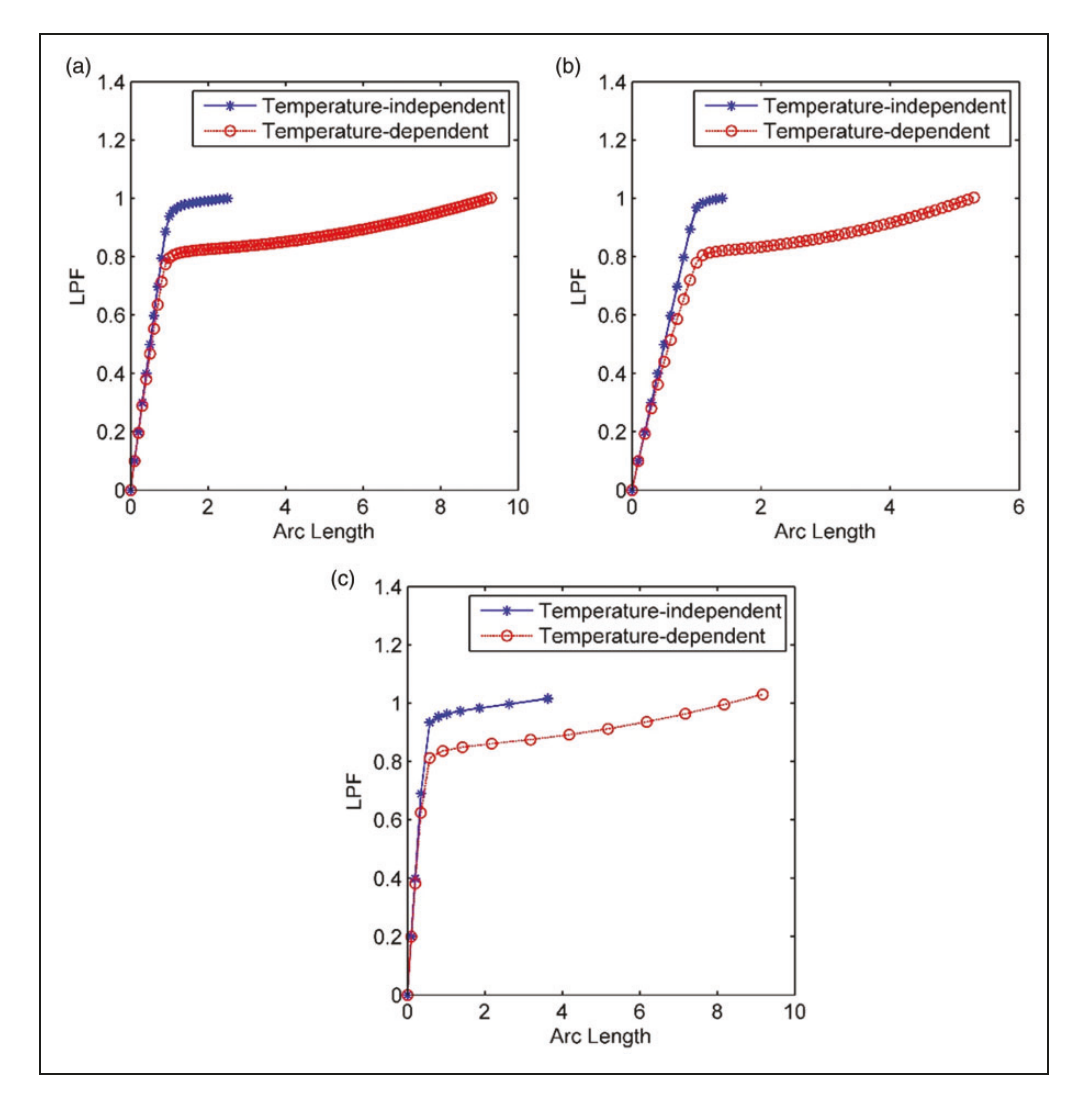


Figure 11. The load history diagrams of models with temperature-dependent coefficients of thermal expansion. (a) Model 1, (b) model 2, and (c) model 3. LPF: load proportionality factor.

temperatures of all three models are around 80% of the values obtained from the linear models. It can be concluded that the expansion coefficients affect the critical buckling temperatures significantly rather than the Young's moduli. The comparisons between the displacement profiles in the axial direction along the outer radius of model 1 and along the inner radius of model 2 at the critical buckling temperatures as well as at the temperatures $100\,^{\circ}\mathrm{C}$ above the critical buckling temperatures are shown in Figure 13.

From Figure 13, it is found that at the critical buckling temperature the maximum displacement along the outer radius of model 1 increases from 0.3 to 1.6 mm, and at 100 °C above the critical buckling temperature the maximum displacement along the outer radius of model 1 increases from 1.7 to 2.6 mm. It is also shown that at the critical

buckling temperature the maximum displacement along the inner radius of model 2 increases from 0.2 to 1.9 mm, and at 100 °C above the critical buckling temperature the maximum displacement along the inner radius of model 2 increases from 2.1 to 2.5 mm.

The displacement profiles in the axial direction along the radius of model 3 with temperature-dependent material properties at the critical buckling temperature and 100 °C above the critical buckling temperature are shown in Figure 14. It indicates that at the critical buckling temperature the largest displacement at the inner radius of model 3 increases from 0.4 to 1.1 mm, and at 100 °C above the critical buckling temperature the largest displacement at the inner radius of model 3 increases from 1.1 to 1.6 mm.

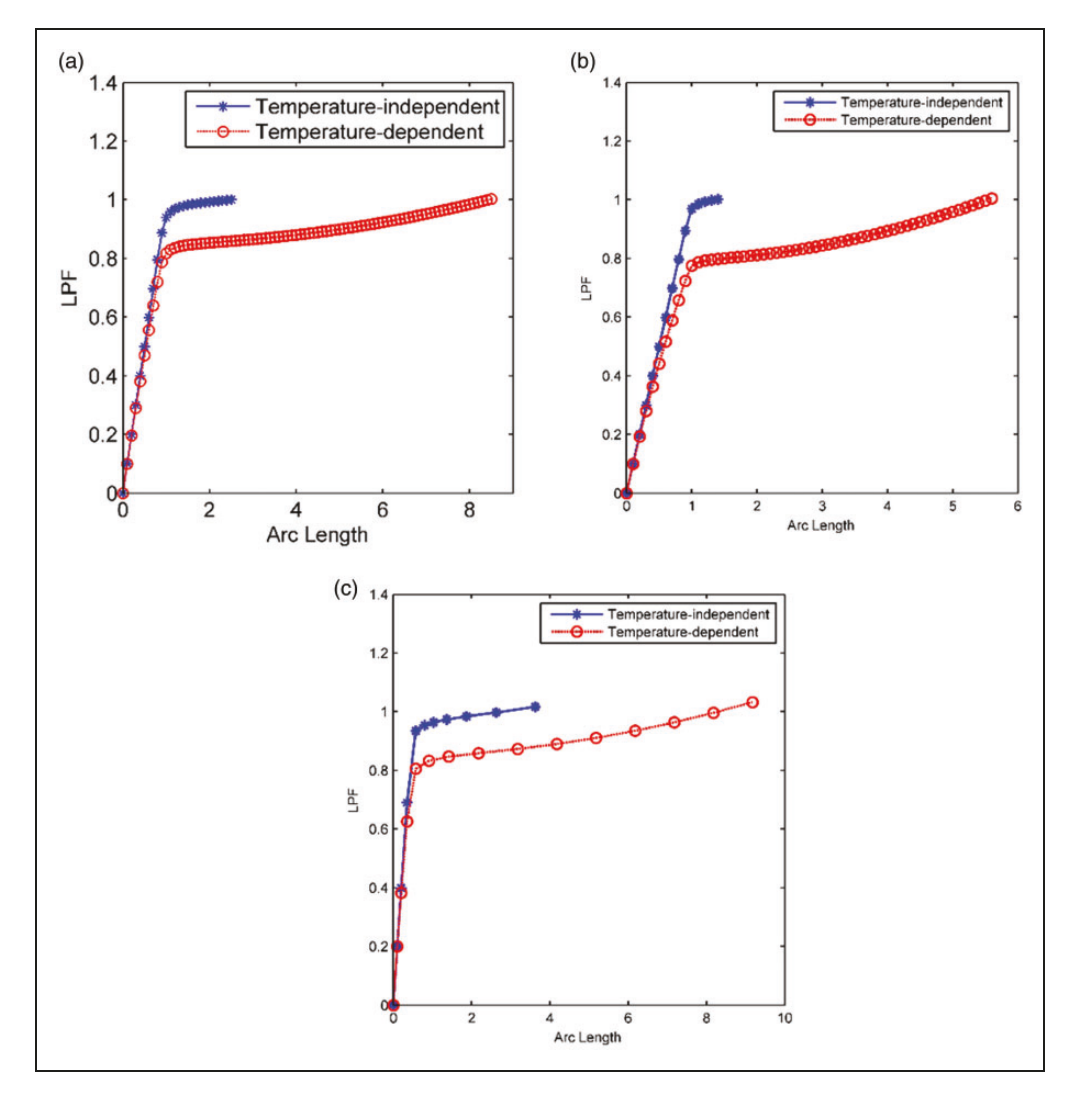


Figure 12. The load history diagrams of models with temperature-dependent elastic moduli and coefficients of thermal expansion. (a) Model 1, (b) model 2, and (c) model 3. LPF: load proportionality factor.

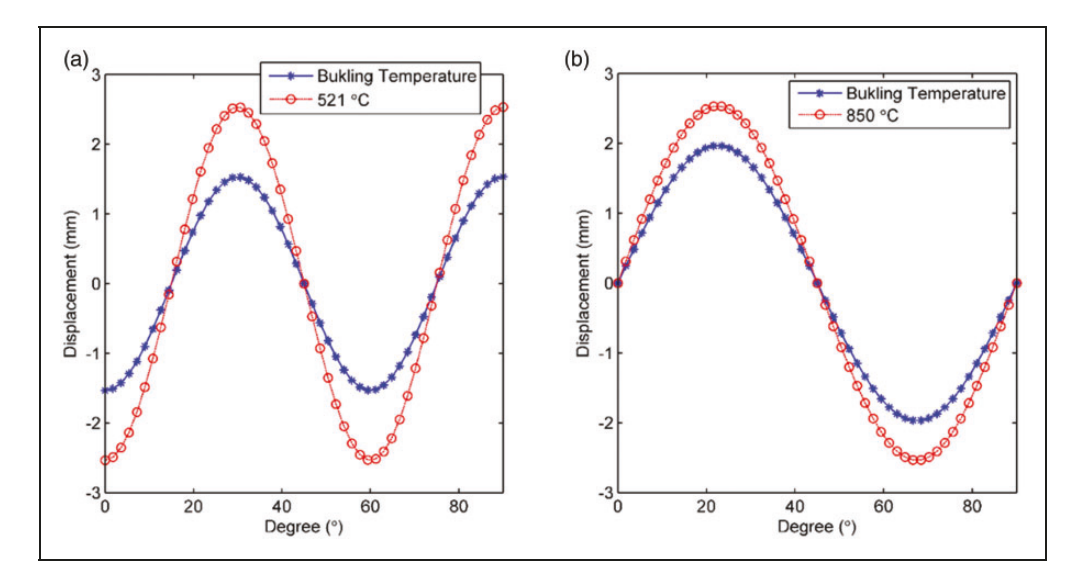


Figure 13. (a) The displacement profiles in the axial direction at the outer radius of model 1 and (b) the displacement profiles in axial direction at the inner radius of model 2.

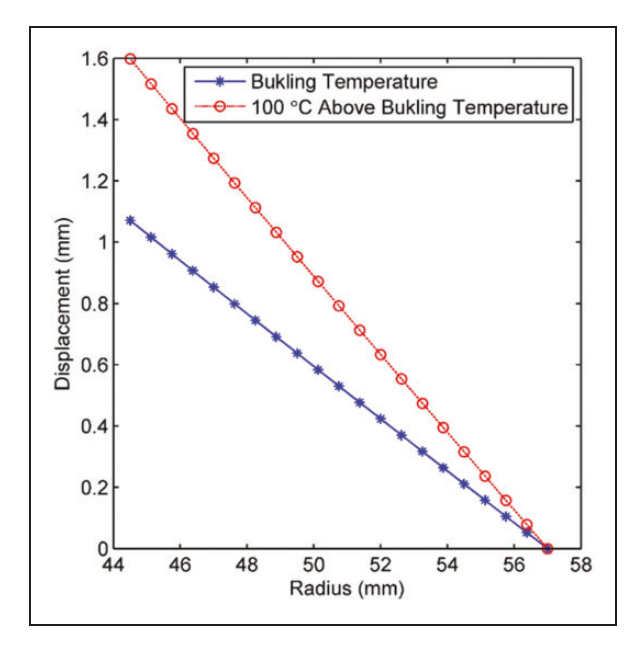


Figure 14. The displacement in the axial direction along the radius of model 3.

Conclusions

Multiple finite element models have been developed to evaluate the postbuckling characteristics of clutch metal disks or any other ring-shaped mechanical components subjected to elevated temperature. There are two steps involved in the current study. The first step is developing linear buckling models to obtain the critical buckling temperatures and the associated buckling deformation modes. The displacement fields extracted from the deformed shapes are imported to the original geometries to generate the perturbed meshes used in the second step. The second step is developing the nonlinear buckling FEA models to investigate the postbuckling behaviors. In the current study, the linearly distributed temperature fields are assumed as the reference loads for the linear buckling analyses. The effects of the temperature-dependent material properties are also investigated. It has been found that for temperaturedependent elastic modulus and temperature-independent coefficient of thermal expansion, the change in the buckling temperature is insignificant. However, the critical buckling temperature could decrease significantly when the expansion coefficient is temperature-dependent. Therefore, a linear buckling analysis assuming constant material properties is insufficient. In addition, it is revealed that the maximum displacements during postbuckling can be increased when the material properties are temperature-dependent.

Declaration of Conflicting Interests

The author(s) declared no potential conflicts of interest with respect to the research, authorship, and/or publication of this article.

Funding

The author(s) disclosed receipt of the following financial support for the research, authorship, and/or publication of this article: This work was supported by the Foundation of Henan University of Technology [grant number: 2019BS015]; the National Science Foundation of China [grant number: NSFC 51405455]; and the National Science Foundation [grant number: NSF 1928876].

ORCID iD

Zhuo Chen https://orcid.org/0000-0003-2513-2758

References

- 1. Zagrodzki P. Numerical analysis of temperature fields and thermal stresses in the friction discs of a multidisc wet clutch. *Wear* 1985; 101: 255–271.
- Audebert N, Barber J and Zagrodzki P. Buckling of automatic transmission clutch plates due to thermoelastic/plastic residual stresses. *J Therm Stresses* 1998; 21: 309–326.
- 3. Ma C. *Thermal buckling of automotive brake discs*. PhD Dissertation, University of Michigan, USA, 2004.
- Xiong C, Ma B, Li H, et al. Experimental study and thermal analysis on the buckling of friction components in multi-disc clutch. *J Therm Stresses* 2015; 38: 1323–1343.
- Najafizadeh M and Hedayati B. Refined theory for thermoelastic stability of functionally graded circular plates. J Therm Stresses 2004; 27: 857–880.
- Najafizadeh M and Heydari H. Thermal buckling of functionally graded circular plates based on higher order shear deformation plate theory. Eur J Mech A Solids 2004; 23: 1085–1100.
- 7. Zhao J, Chen Z, Yang H, et al. Finite element analysis of thermal buckling in automotive clutch plates. *J Therm Stresses* 2016; 39: 77–89.
- 8. Chen Z, Yi Y, Bao K, et al. A numerical analysis of the coupling between frictionally excited thermoelastic instability and thermal buckling. *Proc IMechE, Part J: J Engineering Tribology* 2018; 233: 178–187.
- Ma L and Wang T. Nonlinear bending and post-buckling of a functionally graded circular plate under mechanical and thermal loadings. *Int J Solids Struct* 2003; 40: 3311–3330.
- Li S, Zhang J and Zhao Y. Nonlinear thermomechanical post-buckling of circular FGM plate with geometric imperfection. *Thin Walled Struct* 2007; 45: 528–536.
- Sepahi O, Forouzan M and Malekzadeh P. Thermal buckling and postbuckling analysis of functionally graded annular plates with temperature-dependent material properties. *Mater Des* 2011; 32: 4030–4041.
- Ghiasian S, Kiani Y, Sadighi M, et al. Thermal buckling of shear deformable temperature dependent circular/annular FGM plates. *Int J Mech Sci* 2014; 81: 137–148.
- 13. Cook R, Malkus D, Plesha M, et al. *Concepts and applications of finite element analysis*. 4th ed. New York: John Wiley & Sons, 2001, p.648.
- Dassault Group. Abaqus software user's manual, Abaqus 6.9, 2009.

- 15. Chen Z, Yi Y and Zhao J. Fourier finite element model for prediction of thermal buckling in disc clutches and brakes. *J Therm Stresses* 2016; 39: 1241–1251.
- 16. Wu L. *Shell theory*. 1st ed. Shanghai: Shanghai Jiao Tong University Press, 1989, p.456.
- 17. Muameleci M. Linear and nonlinear buckling analyses of plates using the finite element method. Master Thesis, Linköping University, Sweden, 2017.
- Li W. Buckling and postbuckling analysis of plate with multiple cracks. Master Thesis, Nanjing University of Aeronautics and Astronautics, China, 2014.
- 19. Incropera F, Dewitt D, Bergman F, et al. *Fundamentals* of heat and mass transfer. 6th ed. New York: John Wiley & Sons, 2007, p.116.
- Riks E. An incremental approach to the solution of buckling and snapping problems. *Int J Solids Struct* 1979; 15: 524–551.
- Xu F and Li Q. The design of precision machinery.
 1st ed. Beijing: Tsinghua University Press, 2005, p.564.
- 22. Liu T and Liu M. Theoretical analysis of the relationship between elastic constants of metals and temperature. *Mater Mech Eng* 2014; 38: 85–95.